δf Simulation Studies of the Electron-Ion Two-Stream Instability

Hong Qin, Ronald C. Davidson
and Edward A. Startsev

Plasma Physics Laboratory
Princeton University

Presented at

The 31st ICFA ADBW on Electron Cloud Effects (ECloud'04)

April 19 – April 23, 2004

Napa, California, USA

—Heavy Ion Fusion Virtual National Laboratory —

---

*Research supported by the U.S. Department of Energy.

- In the absence of background electrons, an intense ion beam supports collective oscillations (sideband oscillations) with phase velocity ω/k_z upshifted and downshifted relative to the average beam velocity $\beta_b c$.

- Introduction of an (unwanted) electron component (produced, for example, by secondary emission of electrons due to the interaction of halo ions with the chamber wall) provides the free energy to drive the classical two-stream instability.

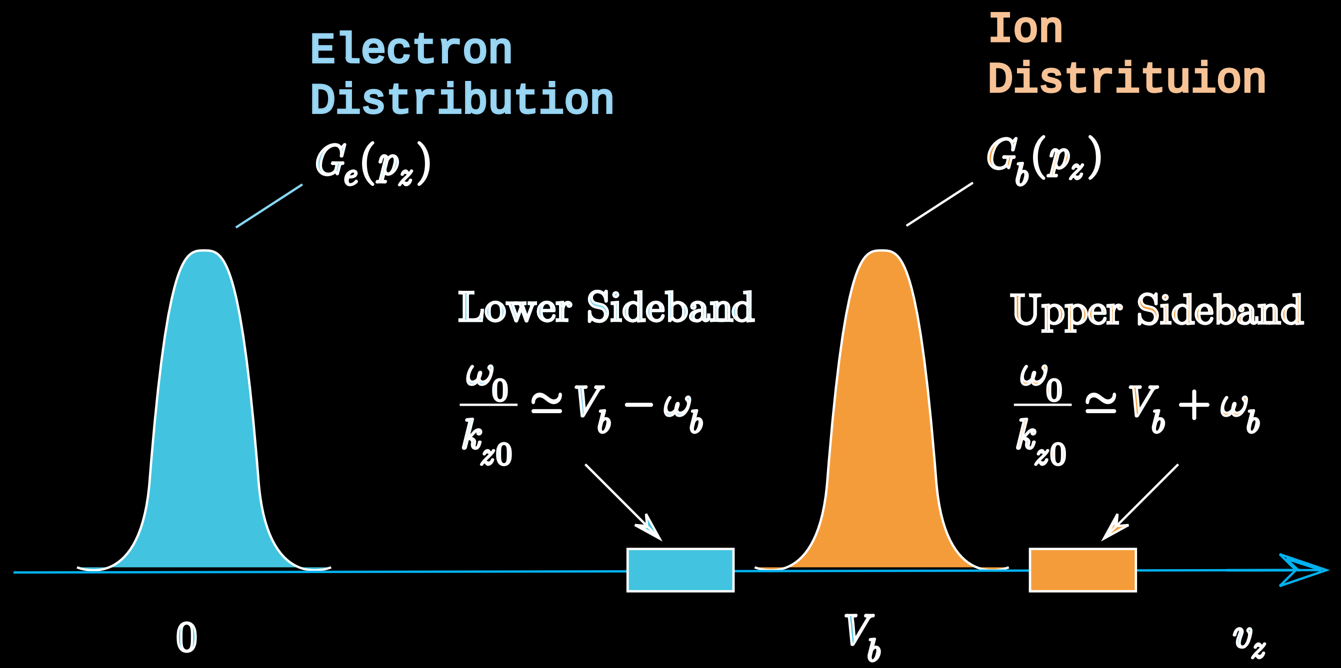

Two-Stream Instability for Intense Ion Beam

- Unlike the two-stream instability in a homogeneous neutral plasma, the two-stream instability for an intense, thin ion beam depends strongly on:
  - Transverse dynamics and geometry (r_b/r_w, $k_z r_b$);
  - Degree of charge neutralization ($f = \hat{n}_e/\hat{n}_b$);
  - Spread in transverse betatron frequencies due to nonlinear space-charge potential as well as chromaticity.
  - Axial momentum spread.
- Strong experimental evidence for two-species instabilities.
  - Proton Storage Ring (PSR) at Los Alamos National Laboratory.
  - Beam-ion instability in electron machines.
  - Electron cloud instability in hadron machines.

Motivation

- Understand two-stream interaction process in high-intensity ion beams, and identify optimum operating regimes for:
  - Spallation Neutron Sources;
  - Hadron colliders;
  - Heavy ion fusion.
- One of the objectives in the Integrated Beam Experiment (IBX) proposed by the U.S. Heavy Ion Fusion Virtual National Laboratory is to study collective effects in a space-charge-dominated beam.
  - Two-stream interactions in IBX are expected to be stronger than the two-stream instabilities observed so far in proton machines because of the much larger beam intensity (Cohen, Molvik, Vay, and Stoltz's).
  - K^+ beam with $m = 39.1$ au and kinetic energy $1.72\,\mathrm{MeV}$ in the low energy regime. Line density $N = 1.50 \times 10^{12}/\,\mathrm{m}$; RMS radius $R_b = 1.3\,\mathrm{cm}$; and beam transverse thermal speed $v_{th} = 0.054\beta_b c$. Vacuum phase advance is $\sigma_v = 72^\circ$, and the applied betatron frequency is $\omega_{\beta b} = 1.21 \times 10^7\,\mathrm{s}^{-1}$.

Presentation Outline

- ⇨ Theoretical mode — nonlinear Vlasov Maxwell system.
- ⇨ Nonlinear δf particle simulation method.
- ⇨ The Beam Equilibrium Stability and Transport (BEST) code.
- ⇨ Nonlinear properties of stable beam propagation.
- ⇨ Eigenmodes by the BEST code — body modes and surface modes.
- ⇨ Ion-electron two-stream instability for heavy ion fusion beams and the Proton Storage Ring experiment at LANL.
- ⇨ Mechanism of damping and nonlinear saturation.
- ⇨ Conclusions and future work.

⇨ Thin, continuous, high-intensity ion beam $(j = b)$ propagates in the z-direction through background electron and ion components $(j = e, i)$ described by distribution function $f_j(\boldsymbol{x}, \boldsymbol{p}, t)$.

⇨ Transverse and axial particle velocities in a frame of reference moving with axial velocity $\beta_j c \hat{\boldsymbol{e}}_z$ are assumed to be *nonrelativistic*.

⇨ Adopt a *smooth-focusing* model in which the focusing force is described by

$$\boxed{\boldsymbol{F}_j^{foc} = -\gamma_j m_j \omega_{\beta j}^2 \boldsymbol{x}_\perp}$$

⇨ Self-electric and self-magnetic fields are expressed as

$$\boxed{\begin{aligned} \boldsymbol{E}^s &= -\nabla\phi(\boldsymbol{x}, t) \\ \boldsymbol{B}^s &= \nabla \times \boldsymbol{A}_z(\boldsymbol{x}, t)\hat{\boldsymbol{e}}_z \end{aligned}}$$

- Distribution functions and electromagnetic fields are described self-consistently by the nonlinear Vlasov-Maxwell equations in the six-dimensional phase space $(\boldsymbol{x}, \boldsymbol{p})$:

$$\boxed{\left\{\frac{\partial}{\partial t} + \boldsymbol{v}\cdot\frac{\partial}{\partial \boldsymbol{x}} - \left[\gamma_j m_j \omega_{\beta j}^2 \boldsymbol{x}_\perp + e_j\left(\nabla\phi - \frac{v_z}{c}\nabla_\perp A_z\right)\right]\cdot\frac{\partial}{\partial \boldsymbol{p}}\right\} f_j(\boldsymbol{x}, \boldsymbol{p}, t) = 0}$$

and

$$\boxed{\begin{aligned} \nabla^2\phi &= -4\pi\sum_j e_j \int d^3p\, f_j(\boldsymbol{x}, \boldsymbol{p}, t) \\ \nabla^2 A_z &= -\frac{4\pi}{c}\sum_j e_j \int d^3p\, v_z f_j(\boldsymbol{x}, \boldsymbol{p}, t) \end{aligned}}$$

What Is Not in the Theoretical Model?

- Simplified electron physics is adopted which neglects:
  - Secondary electron emission from vacuum chamber.
  - Electron dynamics in quadrupole field.
- With the help of the Hamiltonian averaging techniques, a smooth focusing model is used without the complication of finding a 6D phase space “equilibrium” in a periodic focusing lattice.
- A long coasting beam is considered without bunching effects because the longitudinal wavelength of the unstable mode is much shorter than the bunch length.

Nonlinear δf Particle Simulation Method

- Divide the distribution function into two parts: $f_j = f_{j0} + \delta f_j$.
- f_{j0} is a known solution to the nonlinear Vlasov-Maxwell equations.
- Determine numerically the evolution of the perturbed distribution function $\delta f_j \equiv f_j - f_{j0}$.
- Advance the weight function defined by $w_j \equiv \delta f_j / f_j$, together with the particles' positions and momenta.
- Equations of motion for the particles are given by

$$\boxed{\begin{aligned} \frac{d\boldsymbol{x}_{\perp ji}}{dt} &= (\gamma_j m_j)^{-1} \boldsymbol{p}_{\perp ji}, \\ \frac{dz_{ji}}{dt} &= v_{zji} = \beta_j c + \gamma_j^{-3} m_j^{-1} (p_{zji} - \gamma_j m_j \beta_j c), \\ \frac{d\boldsymbol{p}_{ji}}{dt} &= -\gamma_j m_j \omega_{\beta j}^2 \boldsymbol{x}_{\perp ji} - e_j \left(\nabla\phi - \frac{v_{zji}}{c} \nabla_\perp A_z\right) \end{aligned}}$$

- Weight functions w_j are carried by the simulation particles, and the dynamical equations for w_j are derived from the definition of w_j and the Vlasov equation.

Nonlinear δf Particle Simulation Method

⇨ Weight functions evolve according to

$$\boxed{\begin{aligned} \frac{dw_{ji}}{dt} &= -(1-w_{ji})\frac{1}{f_{j0}}\frac{\partial f_{j0}}{\partial \boldsymbol{p}}\cdot\delta\left(\frac{d\boldsymbol{p}_{ji}}{dt}\right) \\ \delta\left(\frac{d\boldsymbol{p}_{ji}}{dt}\right) &\equiv -e_j(\nabla\delta\phi - \frac{v_{zji}}{c}\nabla_\perp\delta A_z) \end{aligned}}$$

Here, $\delta\phi = \phi - \phi_0$, $\delta A_z = A_z - A_{z0}$, and ($\phi_0$, A_{z0}, f_{j0}) are the equilibrium solutions.

⇨ The perturbed distribution function δf_j is given by the weighted Klimontovich representation

$$\boxed{\delta f_j = \frac{N_j}{N_{sj}}\sum_{i=1}^{N_{sj}} w_{ji}\delta(\boldsymbol{x}-\boldsymbol{x}_{ji})\delta(\boldsymbol{p}-\boldsymbol{p}_{ji})}$$

where N_j is the total number of actual j'th species particles, and N_{sj} is the total number of *simulation* particles for the j'th species.

⇨ Maxwell's equations are also expressed in terms of the perturbed quantities:

$$
\begin{aligned}
\nabla^2 \delta\phi &= -4\pi \sum_j e_j \delta n_j \\
\nabla^2 \delta A_z &= -\frac{4\pi}{c} \sum_j \delta j_{zj} \\
\delta n_j &= \int d^3p\, \delta f_j(\boldsymbol{x}, \boldsymbol{p}, t) = \frac{N_j}{N_{sj}} \sum_{i=1}^{N_{sj}} w_{ji} S(\boldsymbol{x} - \boldsymbol{x}_{ji}) \\
\delta j_{zj} &= e_j \int d^3p\, v_z \delta f_j(\boldsymbol{x}, \boldsymbol{p}, t) = \frac{e_j N_j}{N_{sj}} \sum_{i=1}^{N_{sj}} v_{zji} w_{ji} S(\boldsymbol{x} - \boldsymbol{x}_{ji})
\end{aligned}
$$

where $S(\boldsymbol{x} - \boldsymbol{x}_{ji})$ represents the method of distributing particles on the grids.

Advantages of the δf method

- Simulation noise is reduced significantly.
  - Statistical noise $\sim 1/\sqrt{N_s}$.
  - To achieve the same accuracy, number of simulation particles required by the δf method is only $(\delta f/f)^2$ times of that required by the conventional PIC method.
- No waste of computing resource on something already known — f_{j0}.
- Moreover, make use of the known (f_{j0}) to determine the unknown (δf_j).
- Study physics effects separately, as well as simultaneously.
- Easily switched between linear and nonlinear operation.
- Especially desirable for two-stream modes in heavy ion fusion drivers because of
  - Extremely large mass ratio, $m_b/m_e \sim 10^5$;
  - Extremely strong space charge, $s_b = \hat{\omega}_{pb}^2/2\gamma_b^2\omega_{\beta b}^2 \to 1$.

Advanced Features of the BEST Code

Application of the 3D multispecies nonlinear δf simulation method to high intensity beams is carried out using the Beam Equilibrium Stability and Transport (BEST) code at the Princeton Plasma Physics Laboratory.

- Algorithm
  - Nonlinear/linear multispecies δf method based on Vlasov-Maxwell equations.
  - Adiabatic field pusher for light particles (electrons).
  - Solves Maxwell's equations in cylindrical geometry.
- Programming
  - Written in Fortran 90/95 and extensively object-oriented.

Advanced Features of the BEST Code

- Diagnostics
  - HDF5 and NetCDF data format for large-scale diagnostics and visualization.
  - Parallel diagnostics using HDF5.
  - Diagnostic tool developed using IDL.
- Parallelization
  - The code has been parallelized using OpenMP and MPI on IBM-SP supercomputer at NERSC.
  - Good parallel scaling on 512 processors.
  - Achieved 2.0×10^{11} ion-steps $+ 4.0 \times 10^{12}$ electron-steps for instability studies.
- Open source and you are welcome to use it.
  - http://nonneutral.pppl.gov/best.htm .

Nonlinear Properties of Equilibrium Beam

- Single-species thermal equilibrium ion beam in a constant focusing field.
- Equilibrium properties depend on the radial coordinate $r = (x^2 + y^2)^{1/2}$.
- Cylindrical chamber with perfectly conducting wall located at $r = r_w$.
- Thermal equilibrium distribution function for the beam ion is given by

$$\boxed{f_{b0}(r, \boldsymbol{p}) = \frac{\hat{n}_b}{(2\pi\gamma_b m_b T_b)^{3/2}} \exp\left[-\frac{H_\perp}{T_b}\right] \times \exp\left[-\frac{(p_z - \gamma_b m_b \beta_b c)^2}{2\gamma_b^3 m_b T_b}\right]}$$

Nonlinear Properties of Stable Beam Propagation

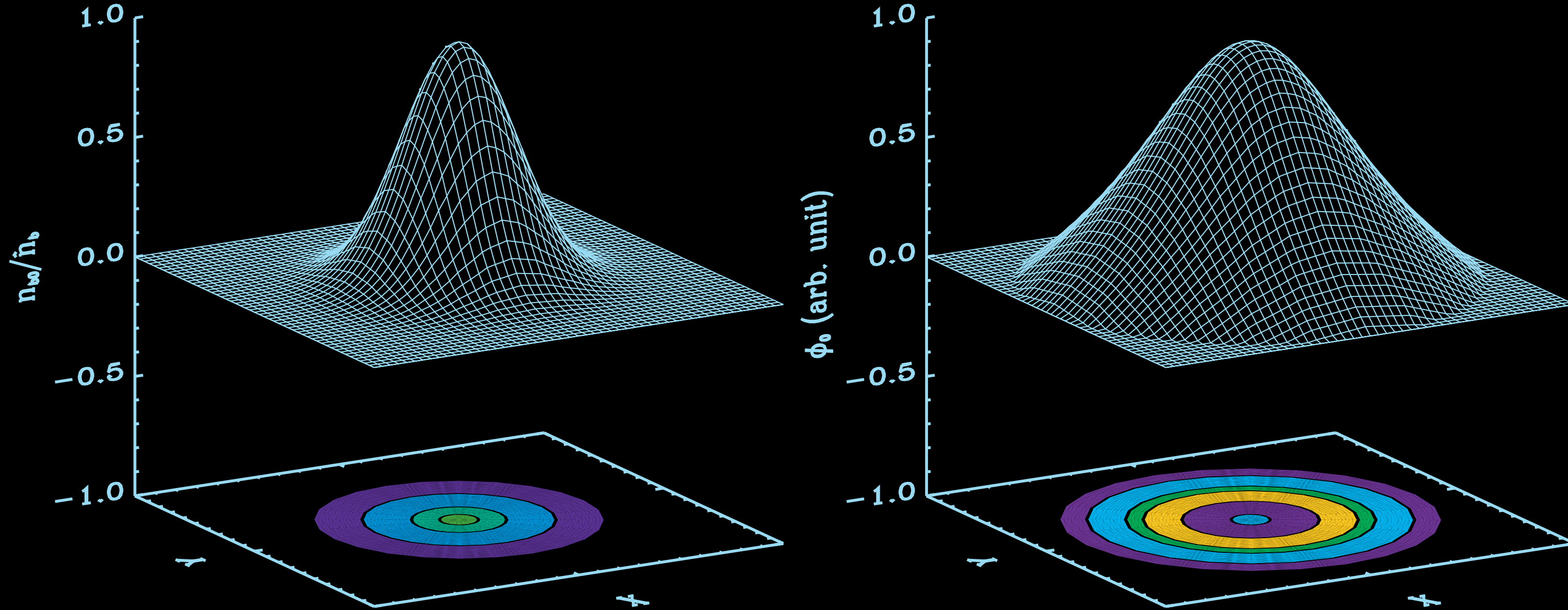

(a) **Equilibrium Density** (b) **Equilibrium Space-Charge Potential**

⇨ Equilibrium solutions (ϕ_0, A_{z0}, f_{j0}) solve the steady-state ($\partial/\partial t = 0$) Vlasov-Maxwell equations with $\partial/\partial z = 0$ and $\partial/\partial\theta = 0$.

Nonlinear Properties of Stable Beam Propagation

⇨ Random initial perturbation with normalized amplitudes of 10^{-3} are introduced into the system.

⇨ The beam is propagated from $t = 0$ to $t = 3000\tau_\beta$, where $\tau_\beta \equiv \omega_{\beta b}^{-1}$.

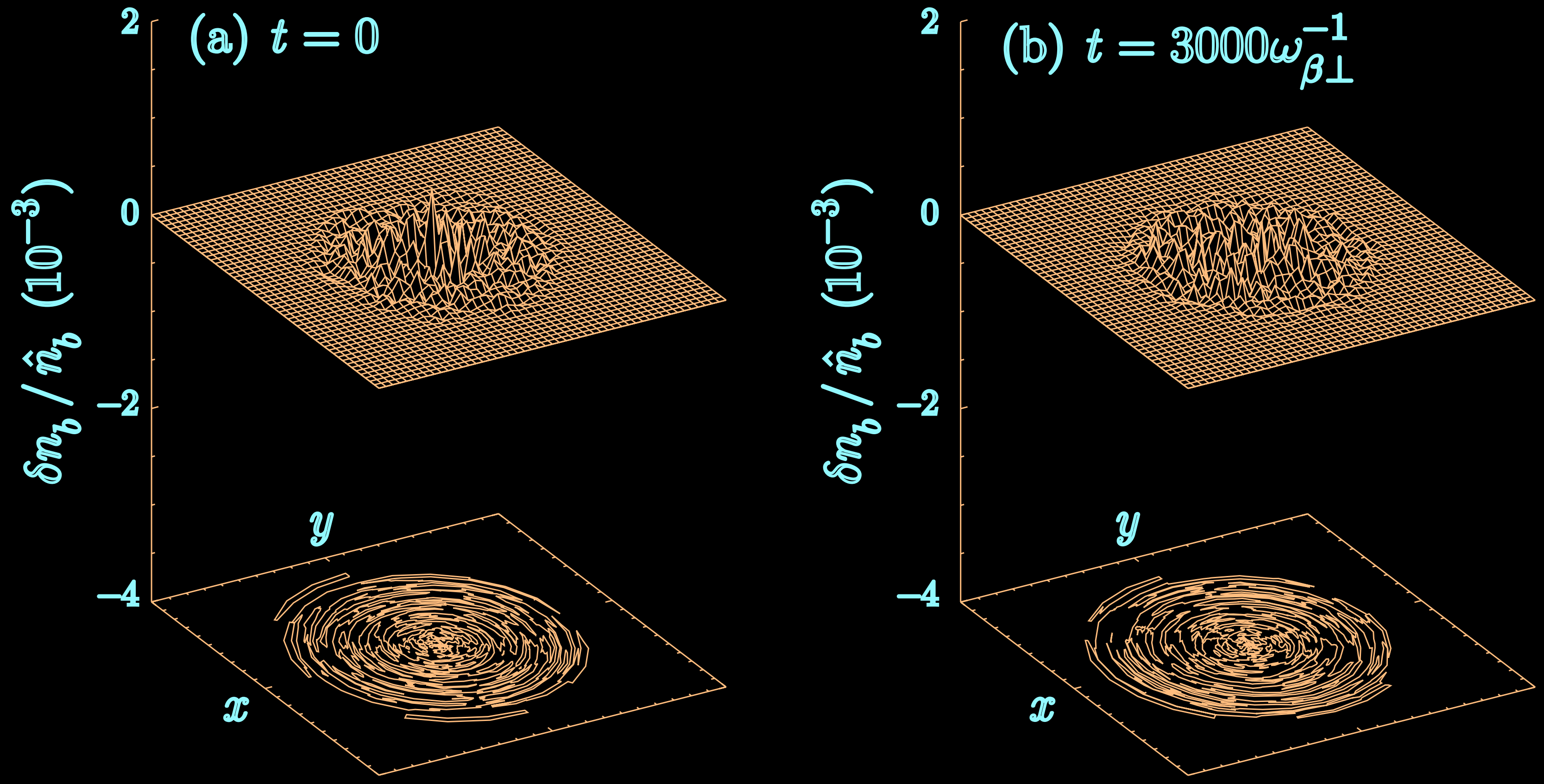

Nonlinear Properties of Stable Beam Propagation

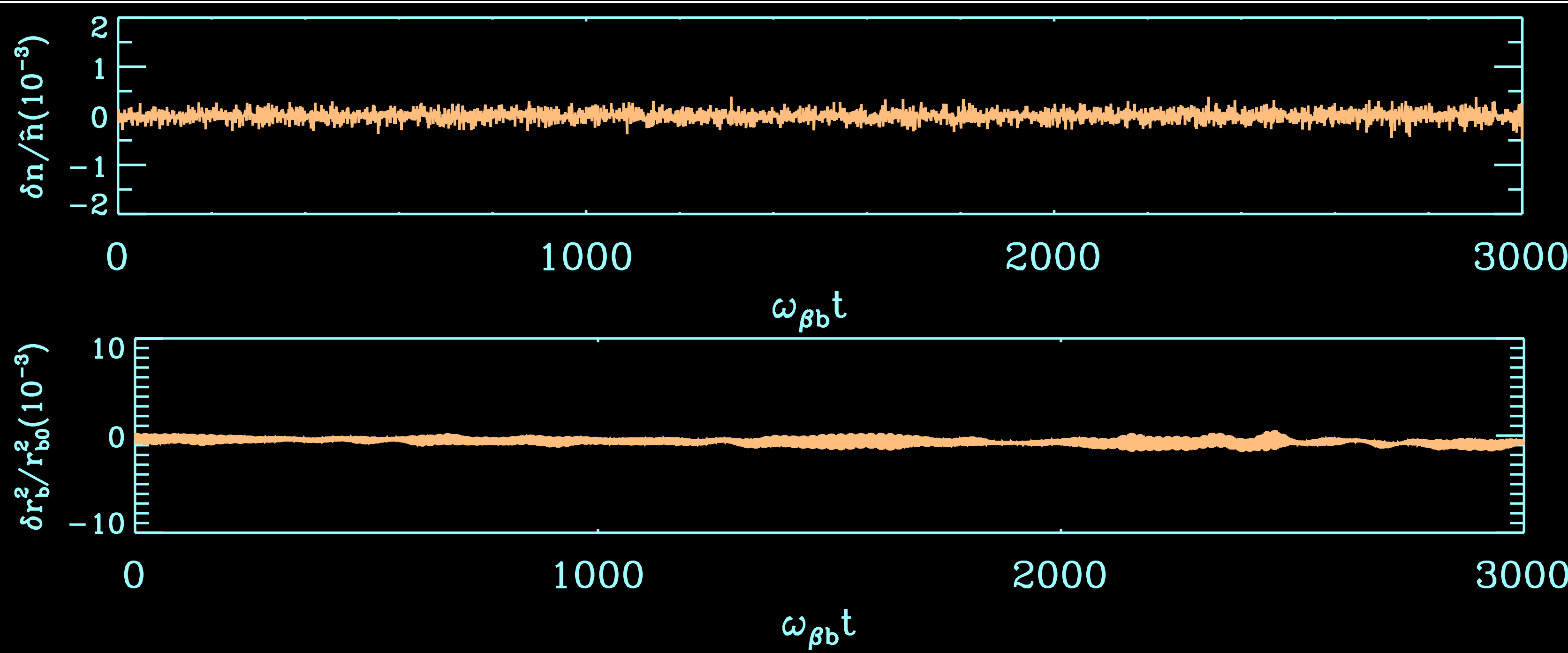

⇨ Simulation results show that the perturbations do not grow and the beam propagates quiescently, which agrees with the nonlinear stability theorem for the choice of thermal equilibrium distribution function [PRL **81**, 991 (1998)].

Axisymmetric Body Modes by the BEST code

- Axisymmetric body modes with $l = 0$ and $k_z = 0$ for a moderate-intensity beam with $s_b \equiv \hat{\omega}_{pb}^2 / 2\gamma_b^2 \omega_{\beta b}^2 = 0.44$.
- First four body eigenmodes of the system at frequencies $\omega_1 = 1.53\ \omega_{\beta b}$, $\omega_2 = 2.98\ \omega_{\beta b}$, $\omega_3 = 4.50\ \omega_{\beta b}$, and $\omega_4 = 6.03\ \omega_{\beta b}$.
- Eigenfunction $\delta\phi_n(r)$ has n zeros when plotted as a function of r.

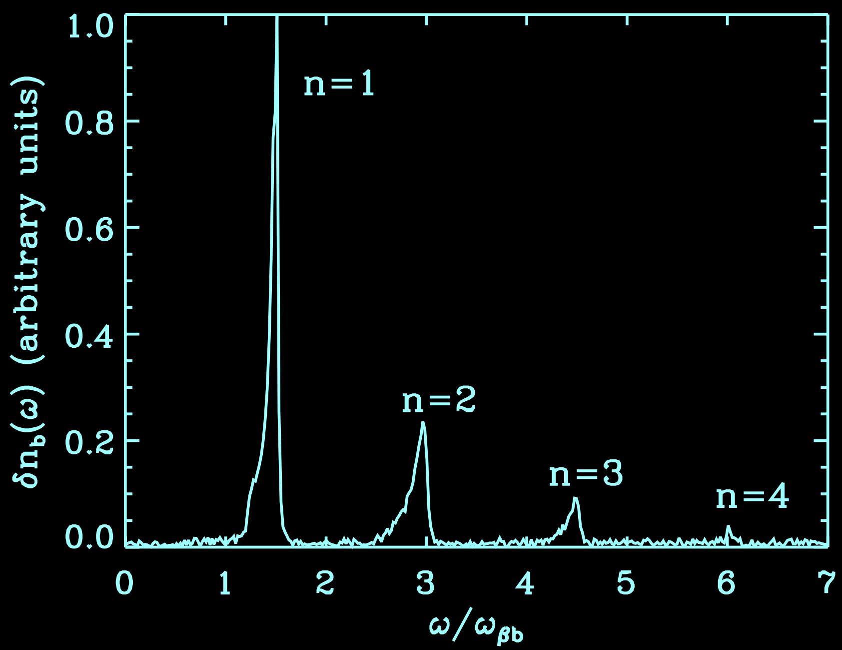

(a) Frequency spectrum

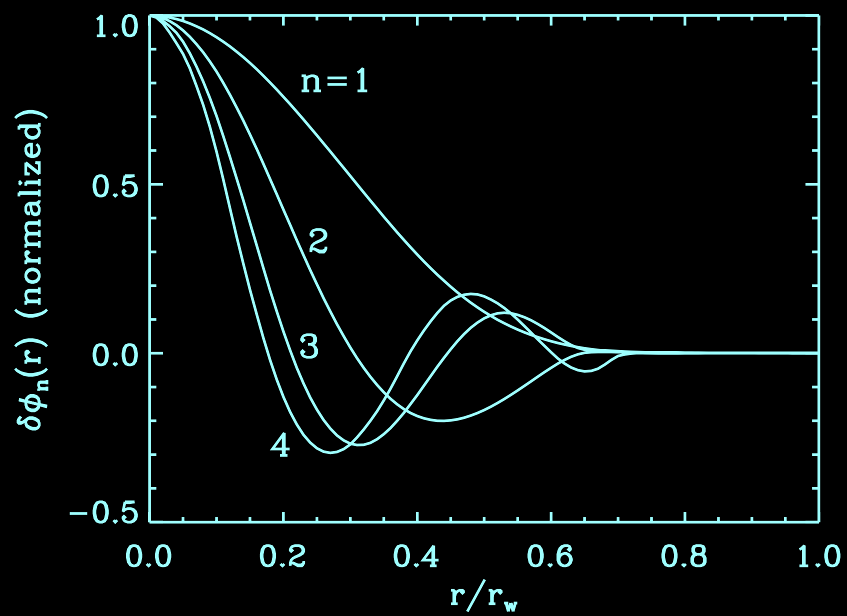

(b) Radial mode structure

Surface Modes

⇨ Linear surface modes for perturbations about a thermal equilibrium beam in the space-charge-dominated regime, with flat-top density profile.

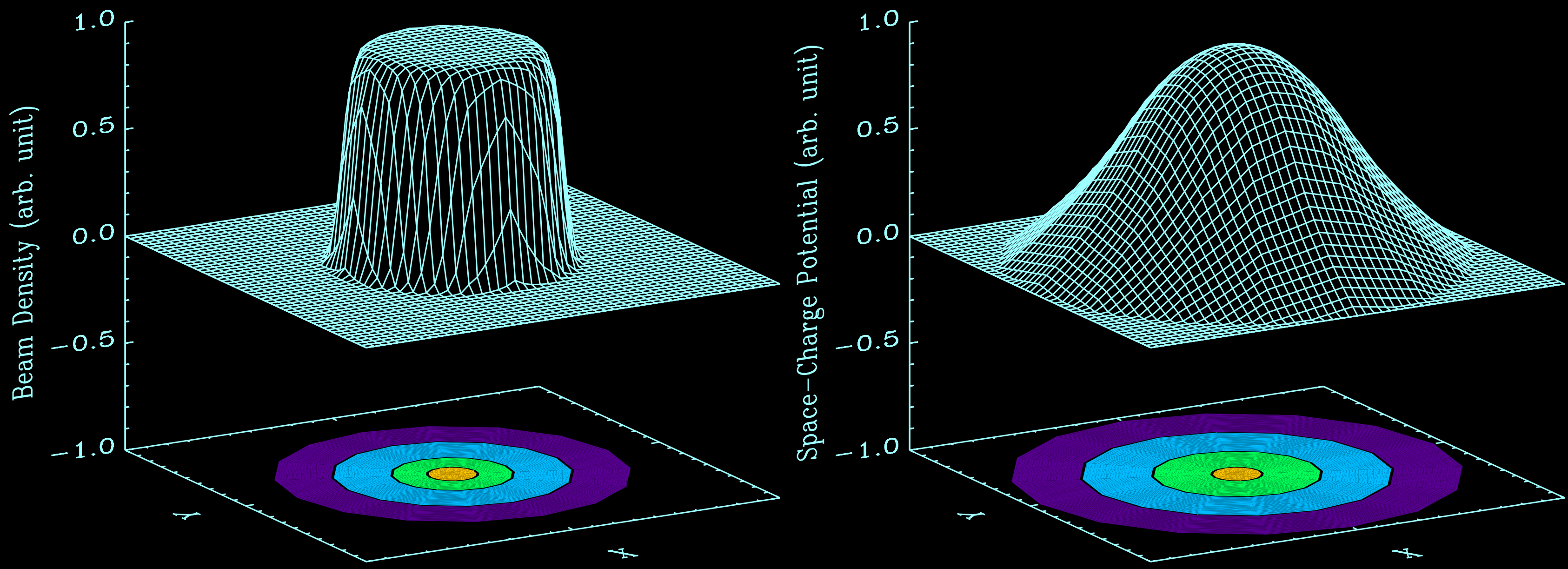

(a) Equilibrium Density

(b) Equilibrium Space-Charge Potential

Surface Modes

- In the absence of background electrons, an intense ion beam supports collective oscillations (sideband oscillations) with phase velocity ω/k_z upshifted and downshifted relative to the average beam velocity $\beta_b c$.

- The BEST code, operating in its linear stability mode, has recovered well-defined eigenmodes which agree with theoretical predications.

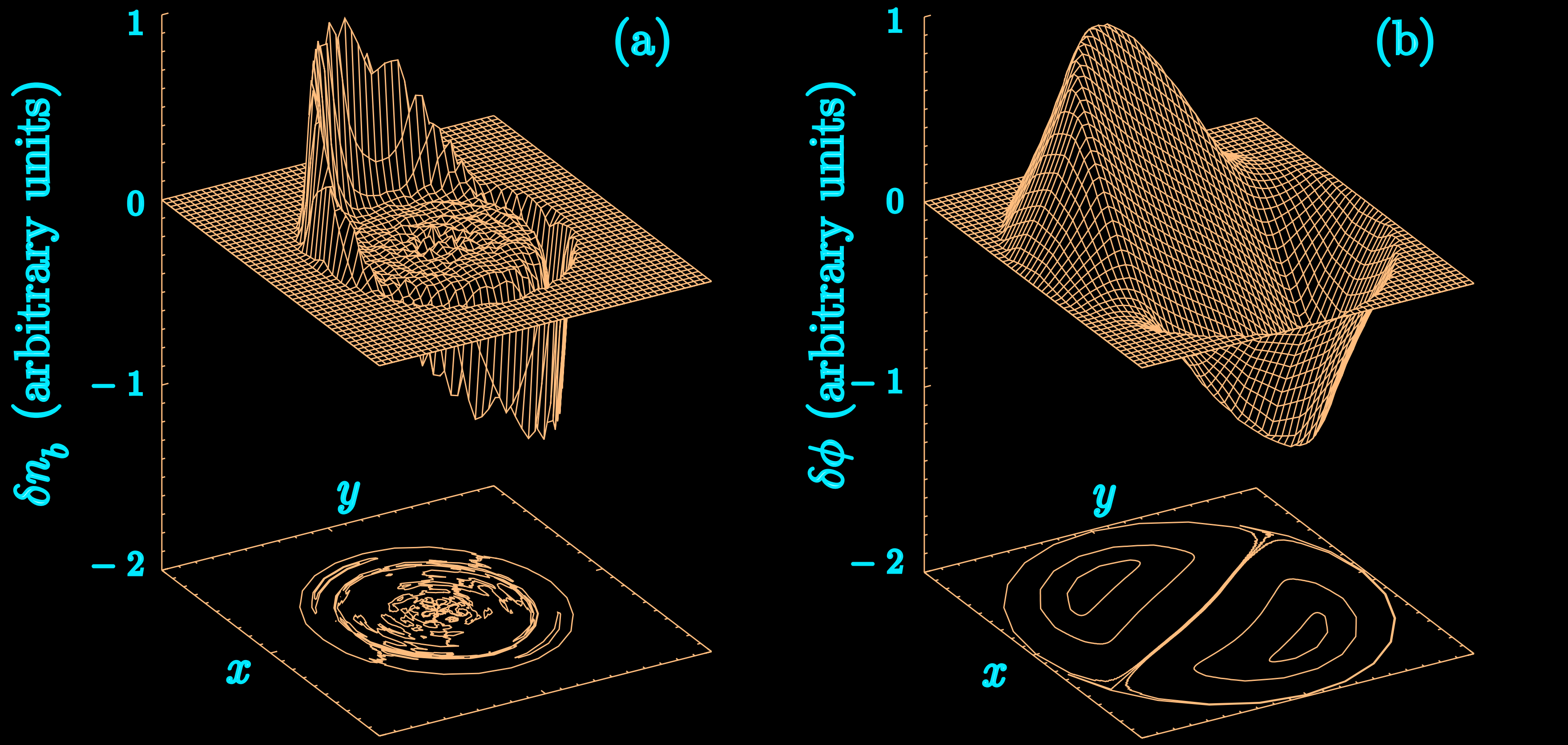

Surface Modes

⇨ For azimuthal mode number $l = 1$, the dispersion relation is given by

$$\boxed{\omega = k_z V_b \pm \frac{\hat{\omega}_{pb}}{\sqrt{2}\gamma_b}\sqrt{1 - \frac{r_b^2}{r_w^2}}}$$

where r_b is the radius of the beam edge, and r_w is location of the conducting wall. Here, $\hat{\omega}_{pb}^2 = 4\pi\hat{n}_b e_b^2/\gamma_b m_b$ is the ion plasma frequency-squared, and $\hat{\omega}_{pb}/\sqrt{2}\gamma_b \simeq \omega_{\beta b}$ in the space-charge-dominated limit.

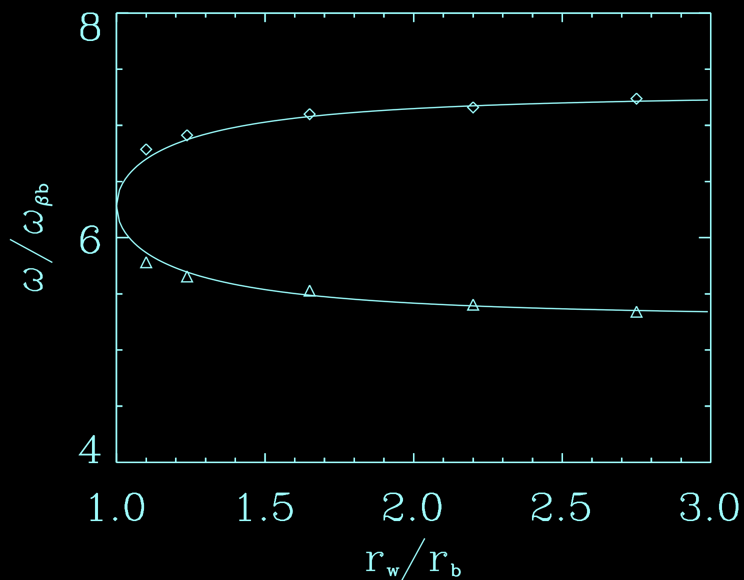

(a) $\omega/\omega_{\beta b}$ **versus** r_w/r_b

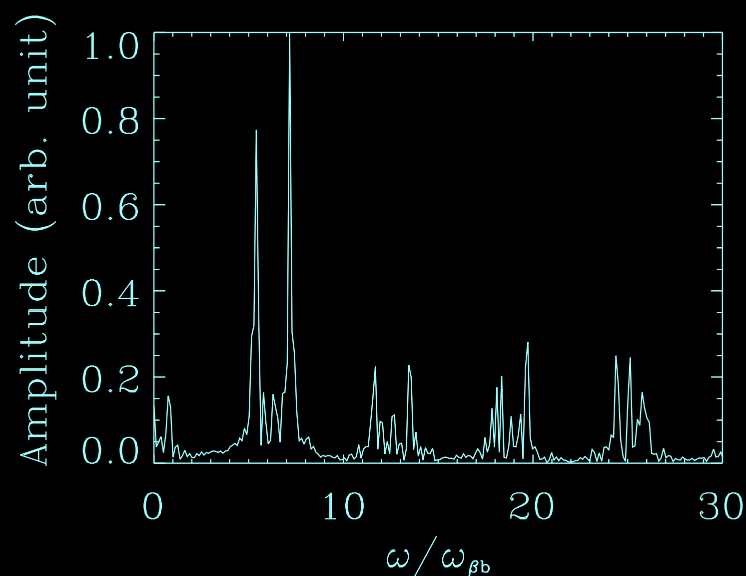

(b) **Spectrum for** $r_w/r_b = 2.2$

- Introduction of an (unwanted) electron component provides the free energy to drive the classical two-stream instability.
- The downshifted surface mode can be destabilized by the ion-electron two-stream interaction when background electrons are present.

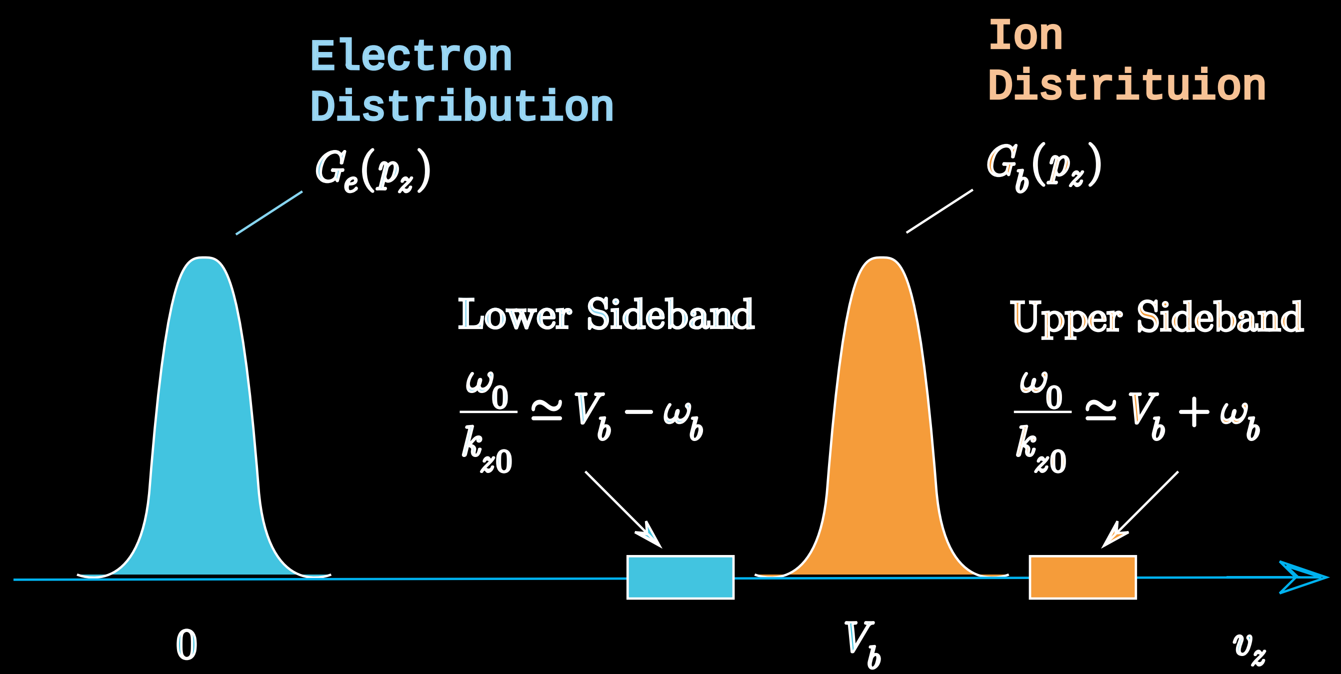

⇨ A careful examination of the kinetic dispersion [Davidson *et al*, 2000] relation shows that the strongest instability occurs for azimuthal mode number $l = 1$ with dispersion relation

$$[(\omega - k_z V_b + i|k_z|v_{T\|b})^2 - \omega_b^2][(\omega + i|k_z|v_{T\|e})^2 - \omega_e^2] = \omega_f^4 \ ,$$

⇨ For $f \neq 0$, the ion and electron modes are coupled by the ω_f^4 term, leading to one unstable mode with $\mathrm{Im}\,\omega > 0$ for a certain range of longitudinal wavenumber k_z.

⇨ The $l = 1$ dipole-mode instability has features similar to the resistive-hose instability in the collisionless limit.

⇨ However, this theoretical model predicts much larger growth rates than those experimentally observed. Significant damping mechanism exist.

⇨ In addition, nonlinear saturation physics are of crucial importance in terms of understanding and control the importance.

Ion-Electron Two-Stream Instability for Illustrative HIF Parameters

- When a background electron component is introduced with $\beta_e = V_e/c \simeq 0$, the $l = 1$ "surface dipole-mode" can be destabilized for a certain range of axial wavenumber and a certain range of electron temperature T_e.

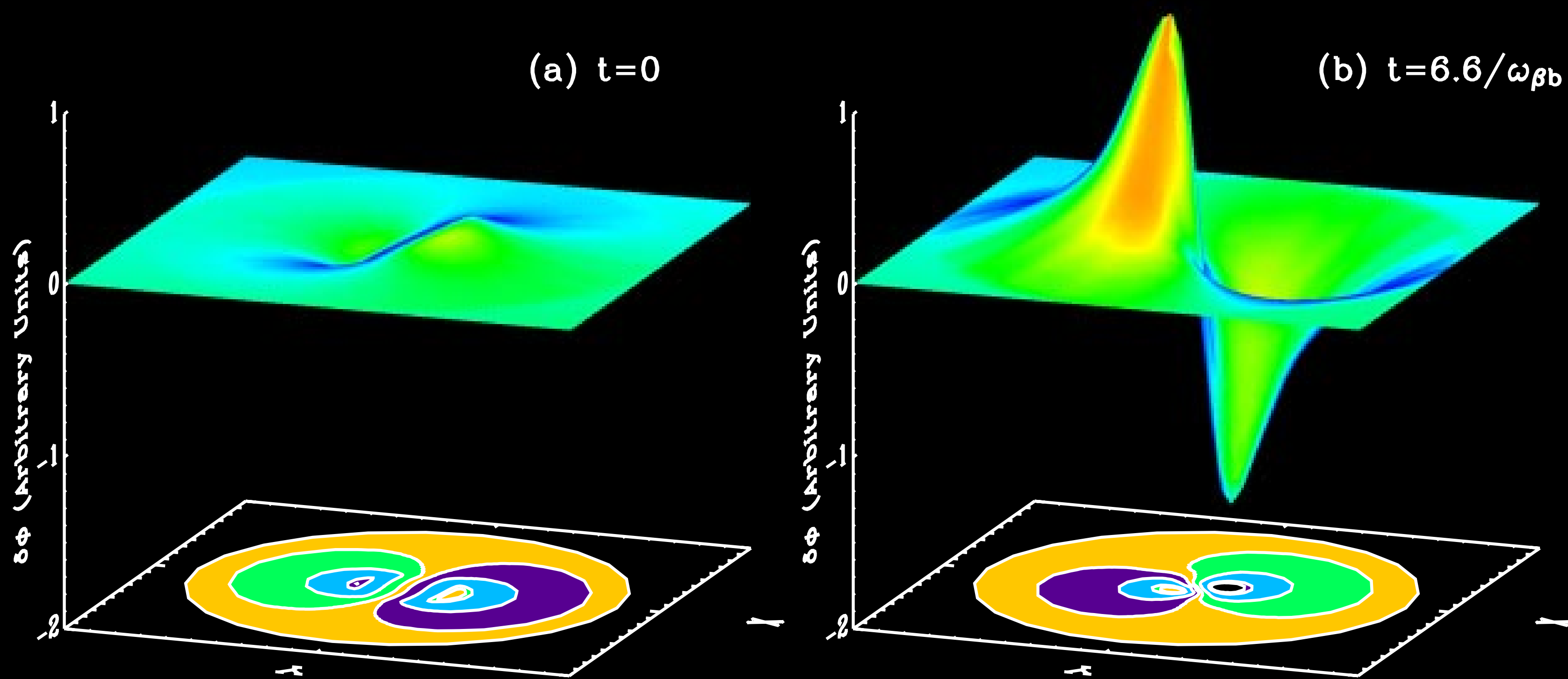

(a) $t = 0$ (b) $t = 6.6/\omega_{\beta b}$

Growth Rate for IBX Parameters

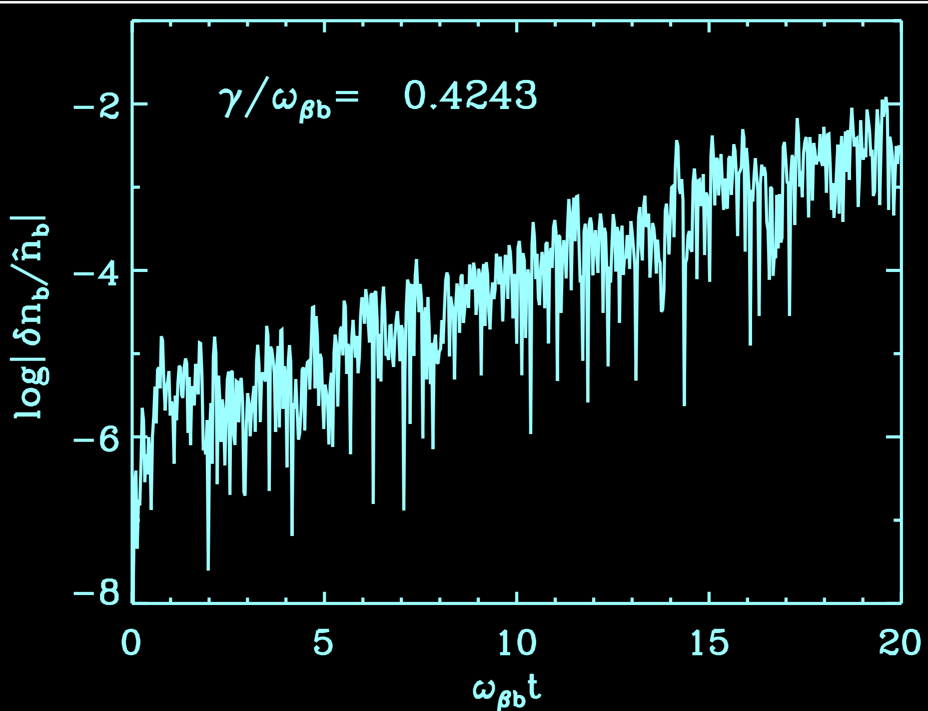

⇨ Illustrative parameters for IBX:

- K^+ beam with rest mass $m_b = 39.1$ au and kinetic energy $(\gamma_b - 1)mc^2 = 1.72$ MeV, $V_e = 0$, and $\omega_{\beta e} = 0$.
- $s_b \equiv \hat{\omega}_{pb}^2/2\gamma_b^2\omega_{\beta b}^2 = 0.996$, $f \equiv \hat{n}_e/\hat{n}_b = 0.05$, where $\hat{n}_e$ and $\hat{n}_b$ are the electron and beam ion densities on axis $(r = 0)$.
- The linear growth rate is measured to be $\mathrm{Im}\,\omega = 0.42\omega_{\beta b}$

Electron-Proton Two-stream Instability in PSR

- ⇨ Proton Storage Ring experiment at Los Alamos is a prototype of the Spallation Neutron Source.
- ⇨ Electron-proton (e-p) two-stream instability was first observed and experimentally studied at the PSR.
- ⇨ Illustrative PSR parameters:
  - Coasting or bunched proton beam with $\gamma_b = 1.85$ in a storage ring of 90m circumference.
  - Moderate space-charge intensity corresponding to $\lambda_b = 9.13 \times 10^8$cm^{-1} or $\hat{\omega}_{pb}^2/2\gamma_b^2\omega_{\beta b}^2 = 0.079$.
  - 10% fractional neutralization, $\lambda_e = 9.25 \times 10^7$cm^{-1}, $T_{b\perp} = 4.41$keV, $T_{e\perp} = 0.73$keV, $\phi_0(r_w) - \phi_0(0) = -3.08 \times 10^3$Volts, and nonlinear space-charge induced tune shift $\delta\nu/\nu_0 \sim -0.020$.
  - Oscillation frequency (simulations): $f \sim 163$MHz. Mode number at maximum growth $n = 55 \sim 65$.

Simulation of the e-p Instability for PSR

- Large-scale parallel simulations using the BEST code has been carried out for the e-p instability in the PSR.

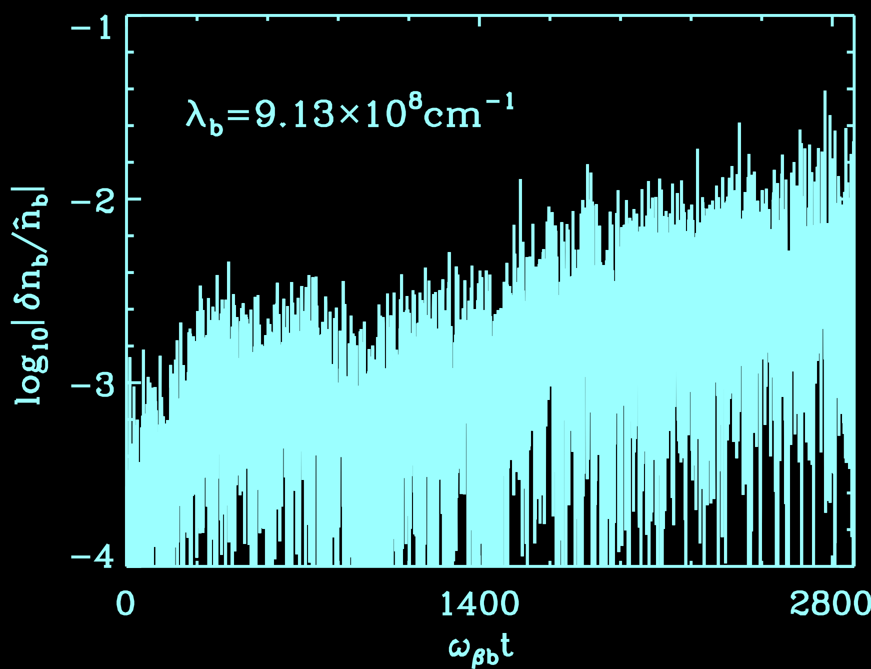

- Simulations results agrees with experimental observations.
  - Characteristic dipole mode structure in unstable linear phase.
  - Mode frequency, growth rate, and wavelength in good agreement.
  - Realistic damping mechanisms in the simulations.
- Late-time nonlinear growth is observed for system parameters above marginal stability.

Damping Mechanism and Nonlinear Saturation

- Damping mechanism and nonlinear saturation are of significant importance.
- Linear (Landau) damping mechanism include those:
  - by momentum spread in longitudinal direction ;
  - by transverse tune spread due to chromaticity;
  - by transverse tune spread due to space charge.
- Nonlinear saturation and secondary growth due to:
  - nonlinearity;
  - wave-particle interaction in the transverse direction;
  - wave-particle interaction in the longitudinal direction;

Landau Damping due to Momentum Spread of Beam Ions (IBX)

⇨ Landau damping by parallel ion kinetic effects provides a damping mechanism that reduces the growth rate.

⇨ The maximum linear growth rate $(\mathrm{Im}\,\omega)_{max}$ of the ion-electron two-stream instability decreases as the longitudinal momentum spread of the beam ions increases.

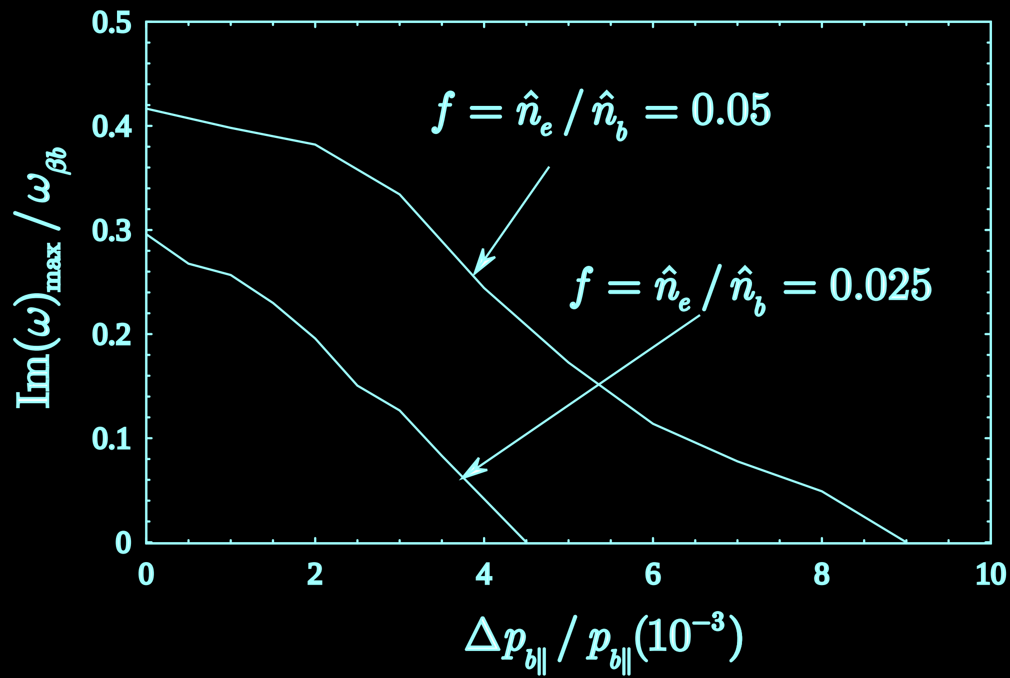

⇨ When $\Delta p_{b\|}/p_{b\|}$ is high enough, the mode is completely stabilized by longitudinal Landau damping effects.

Instability Threshold for Illustrative PSR Parameters

⇨ Maximum growth rate depends on the normalized beam density $\hat{n}_b/\hat{n}_{b0}$ and the initial axial momentum spread.

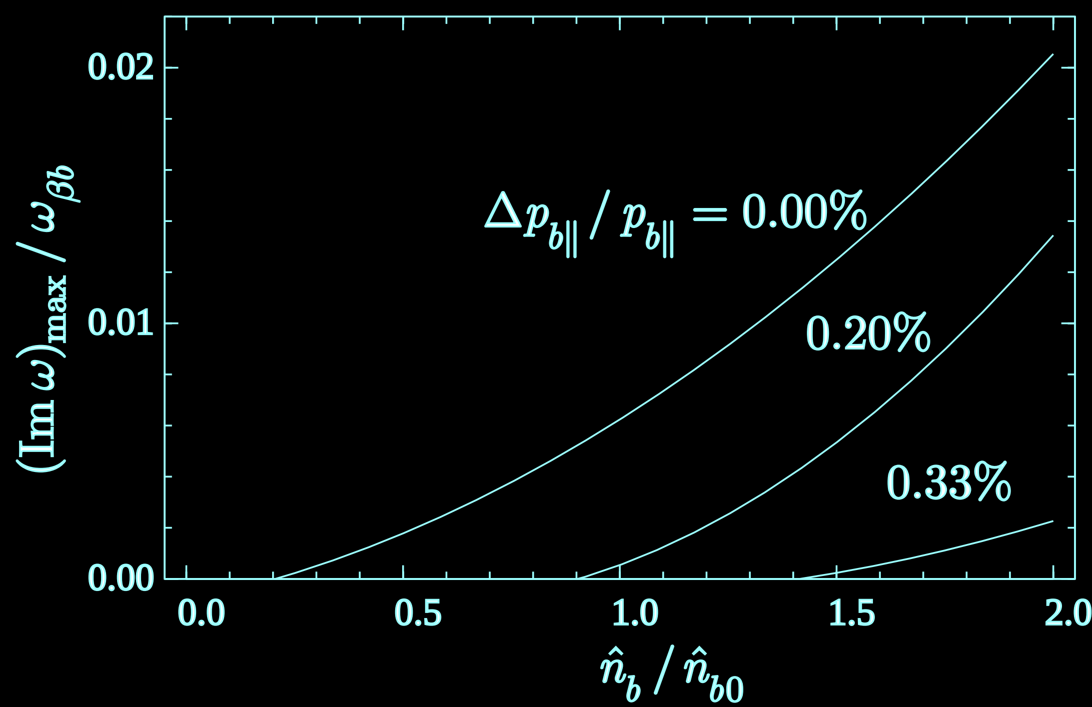

⇨ $\hat{n}_{b0} = 9.41\times10^8 \mathrm{cm}^{-3}$, corresponding to an average current of 35 A ($\hat{\omega}_{pb}^2/2\gamma_b^2\omega_{\beta b}^2 = 0.079$).

⇨ A larger longitudinal momentum spread induces stronger Landau damping by parallel kinetic effects and therefore reduces the growth rate of the instability.

⇨ Higher beam intensity provides more free energy to drive a stronger instability.

Instability Threshold for Illustrative PSR Parameters

- Important damping mechanisms includes
  - Longitudinal Landau damping by the beam ions.
  - Stabilizing effects due to space-charge-induced tune spread.
- An instability threshold is observed in the simulations.

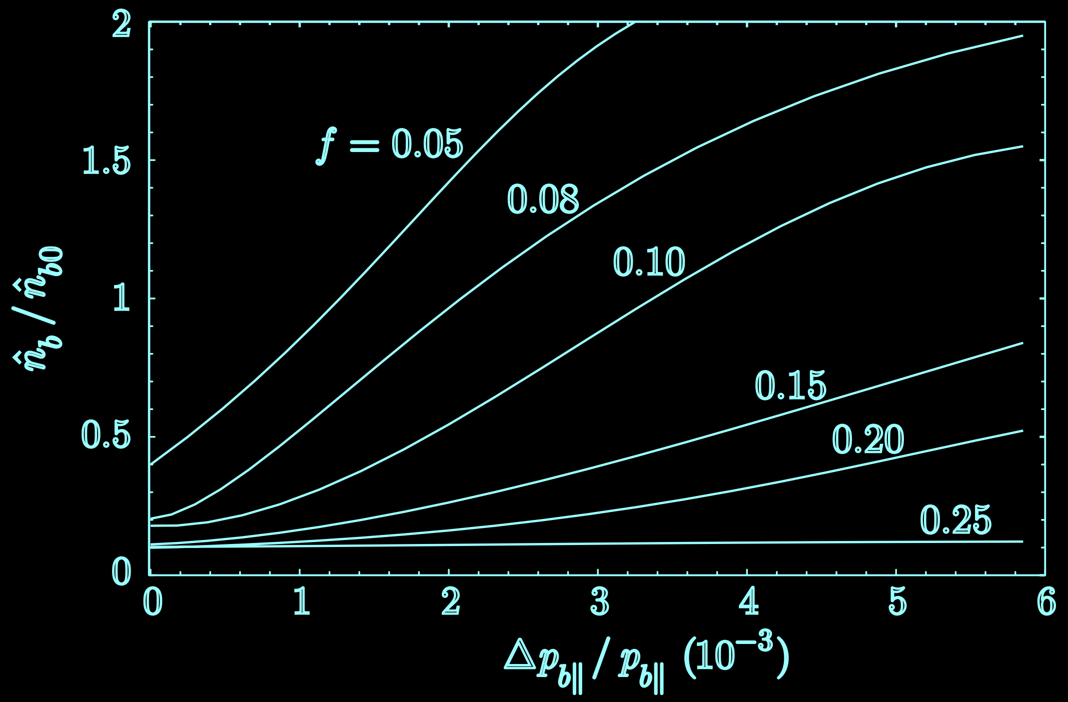

- Larger momentum spread and smaller fractional charge neutralization imply a higher density threshold for the instability to occur.

Space-charge induced tune spread

⇨ Larger tune spread in the transverse direction is induced by higher space-charge intensity.

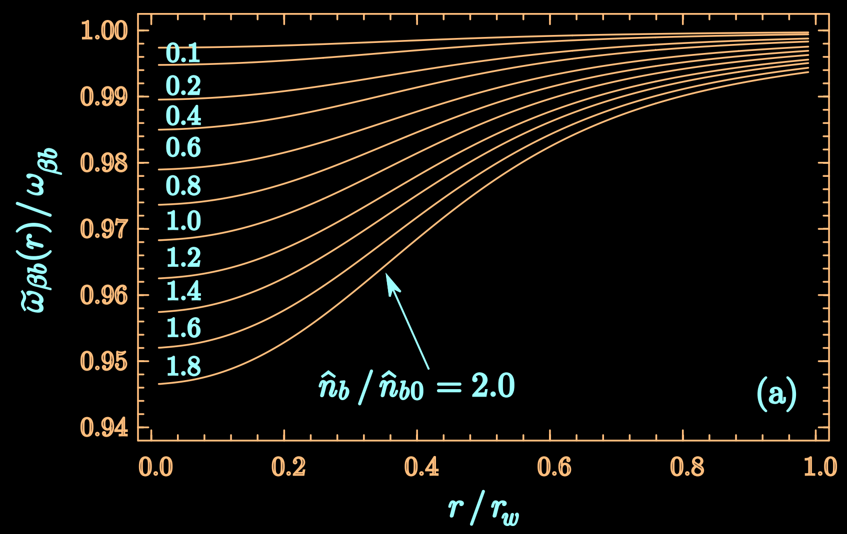

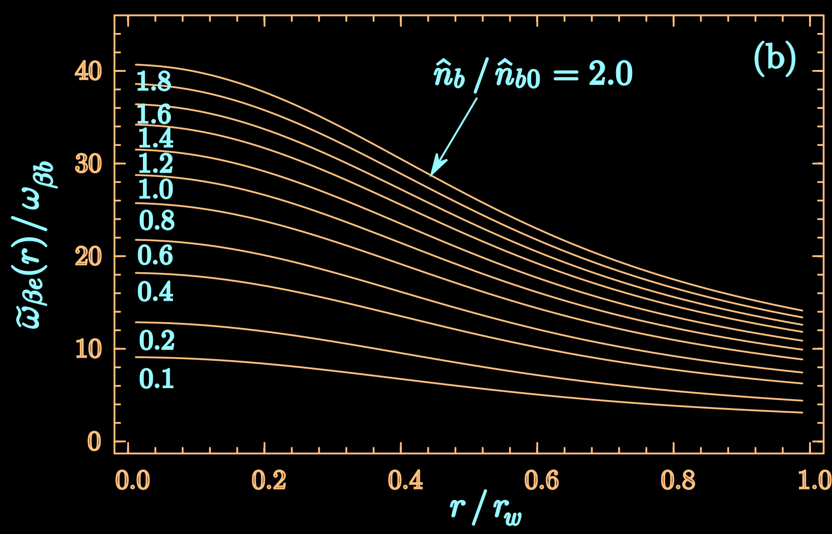

Space-charge induced tune spread

- Larger tune spread in the transverse direction is induced by higher space-charge intensity.

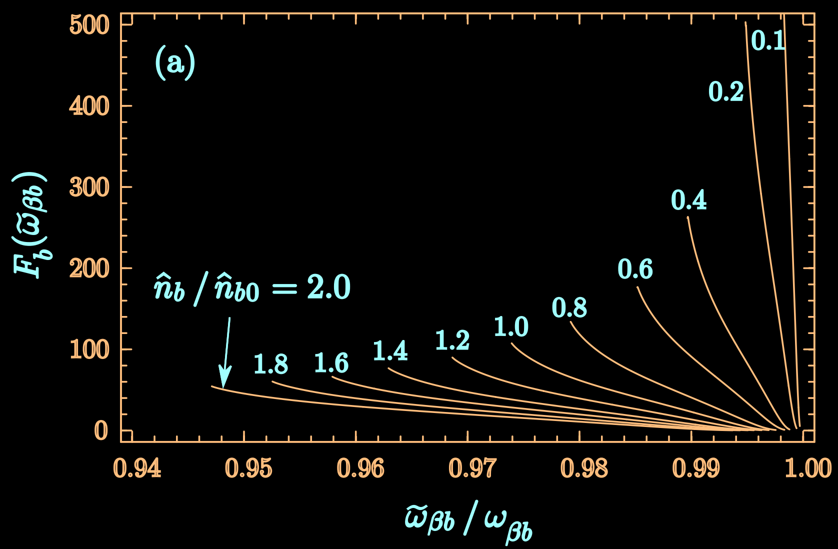

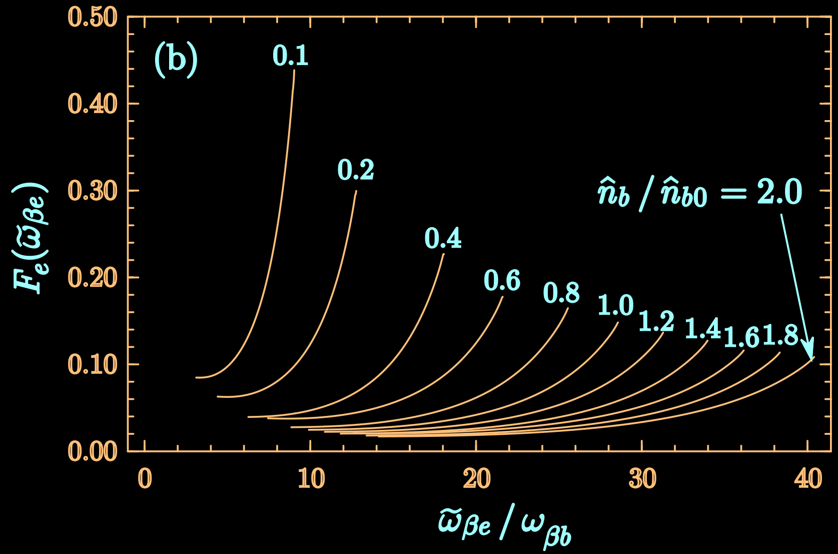

Equilibrium of Ion-Electron Two-Stream System

- Electron population offsets part of the space-charge force.
- Produces bell-shape beam density profile even in the space-charge limit, $s_b = \hat{\omega}_{pb}^2/2\gamma_b^2\omega_{\beta b}^2 \rightarrow 1$.

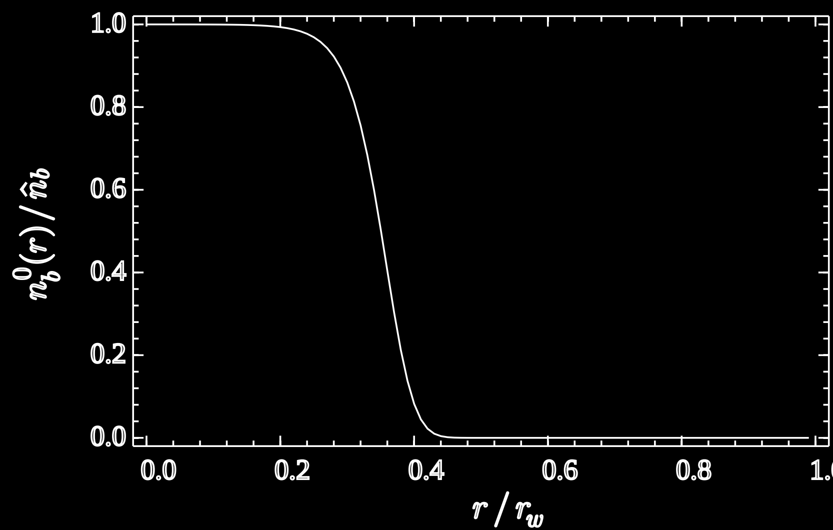

(a) $f = \hat{n}_e/\hat{n}_b = 0$

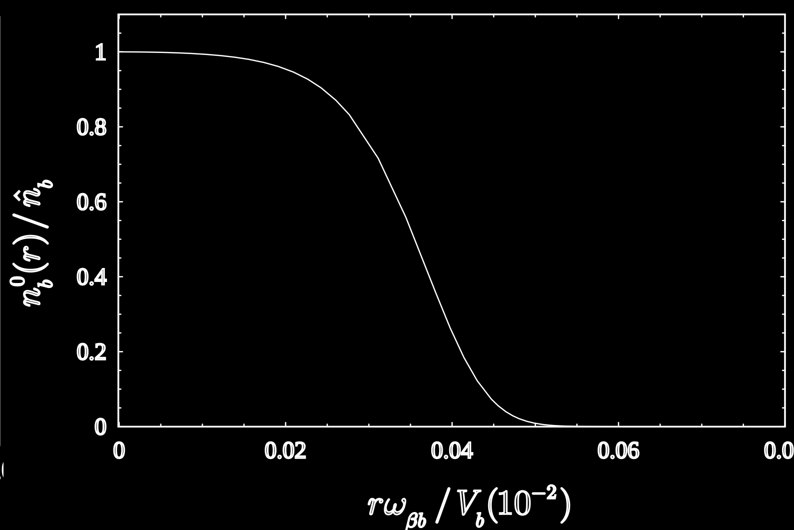

(b) $f = \hat{n}_e/\hat{n}_b = 0.1$

Complex Nonlinear Electron Dynamics During Instability

- Energetic electrons maintain their regular motions.

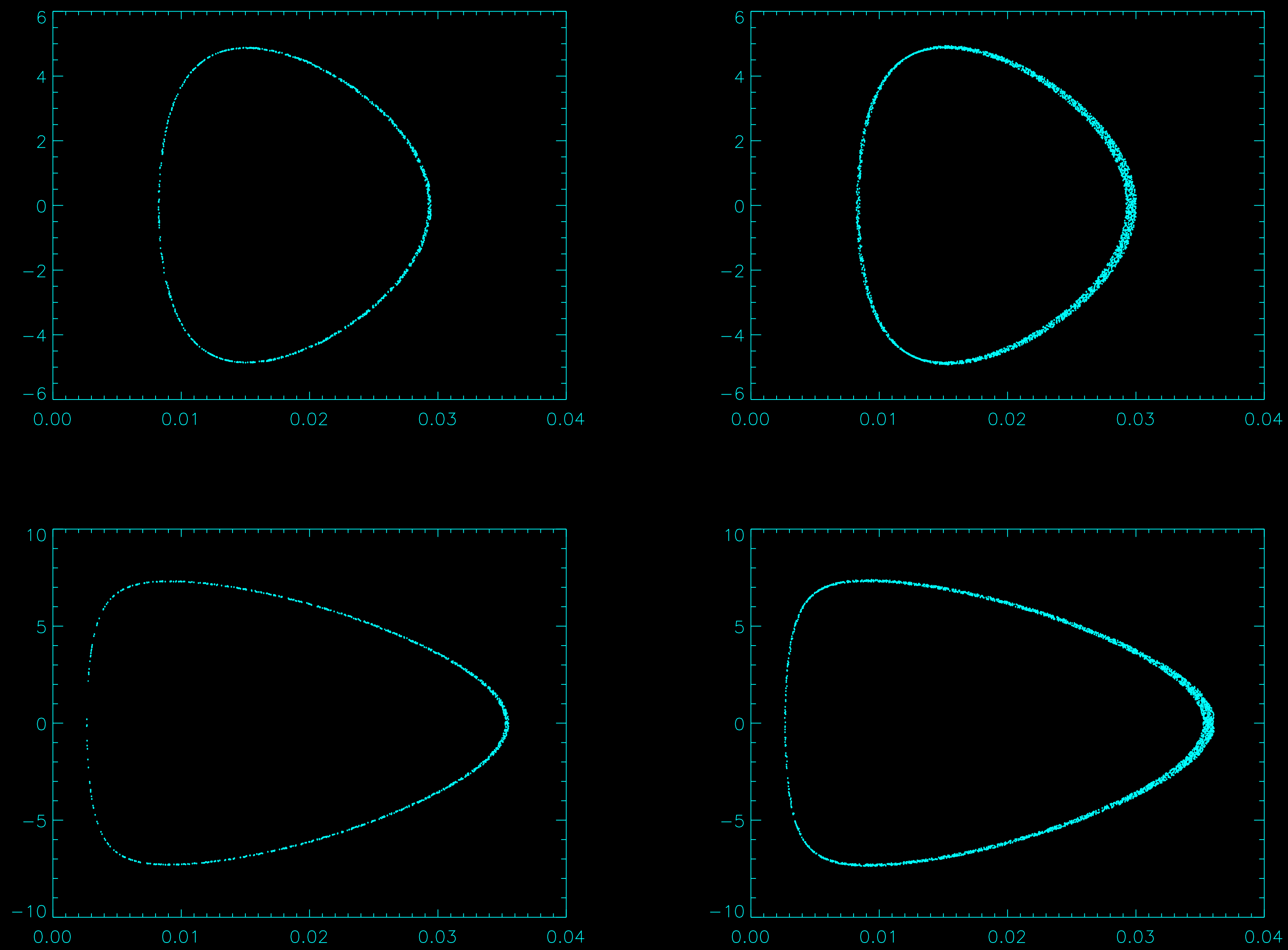

Complex Nonlinear Electron Dynamics During Instability

- Less energetic electrons are influenced by the instability.

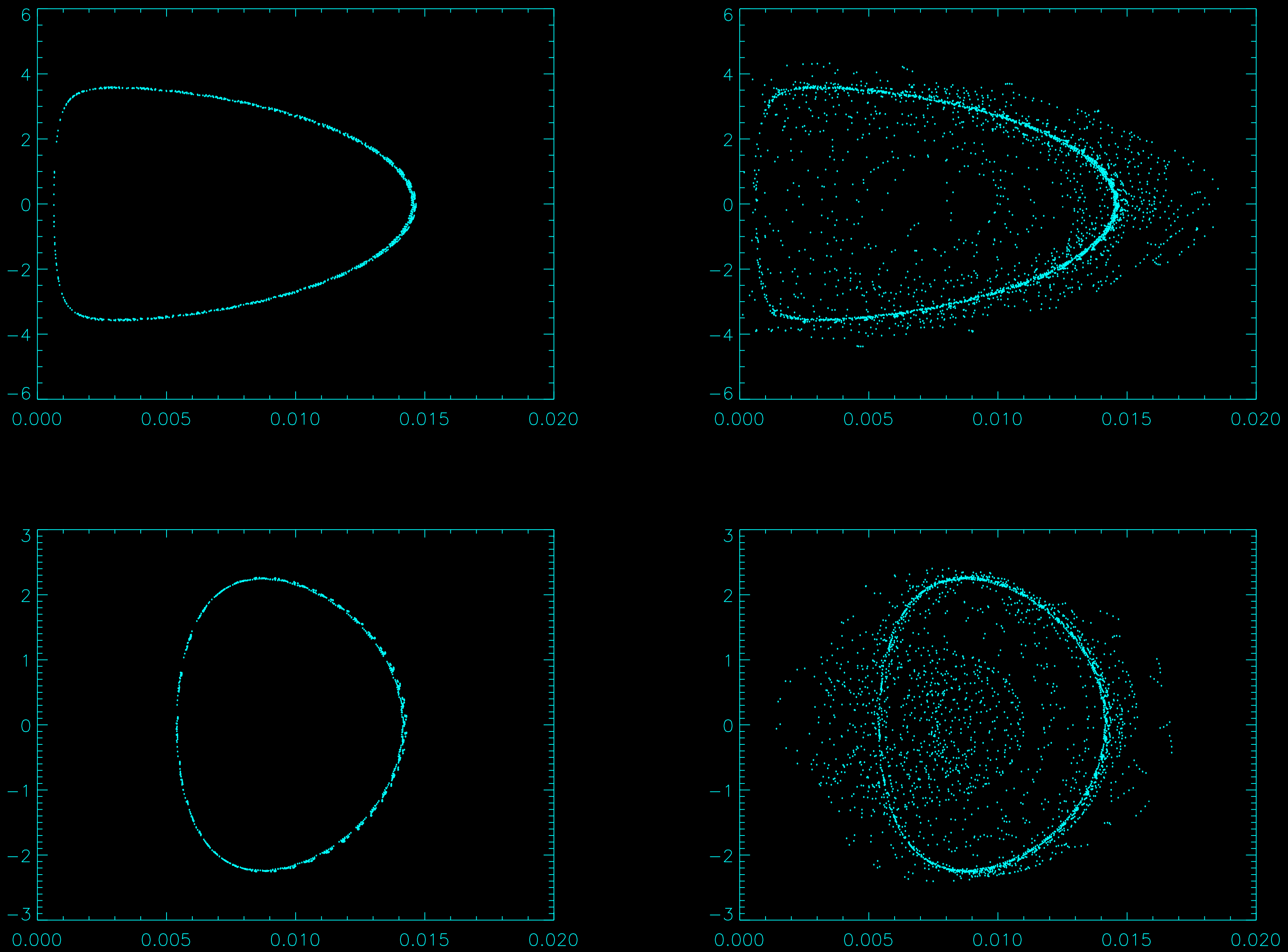

Complex Nonlinear Electron Dynamics During Instability

⇨ Low energy electrons' dynamics become chaotic during the instability.

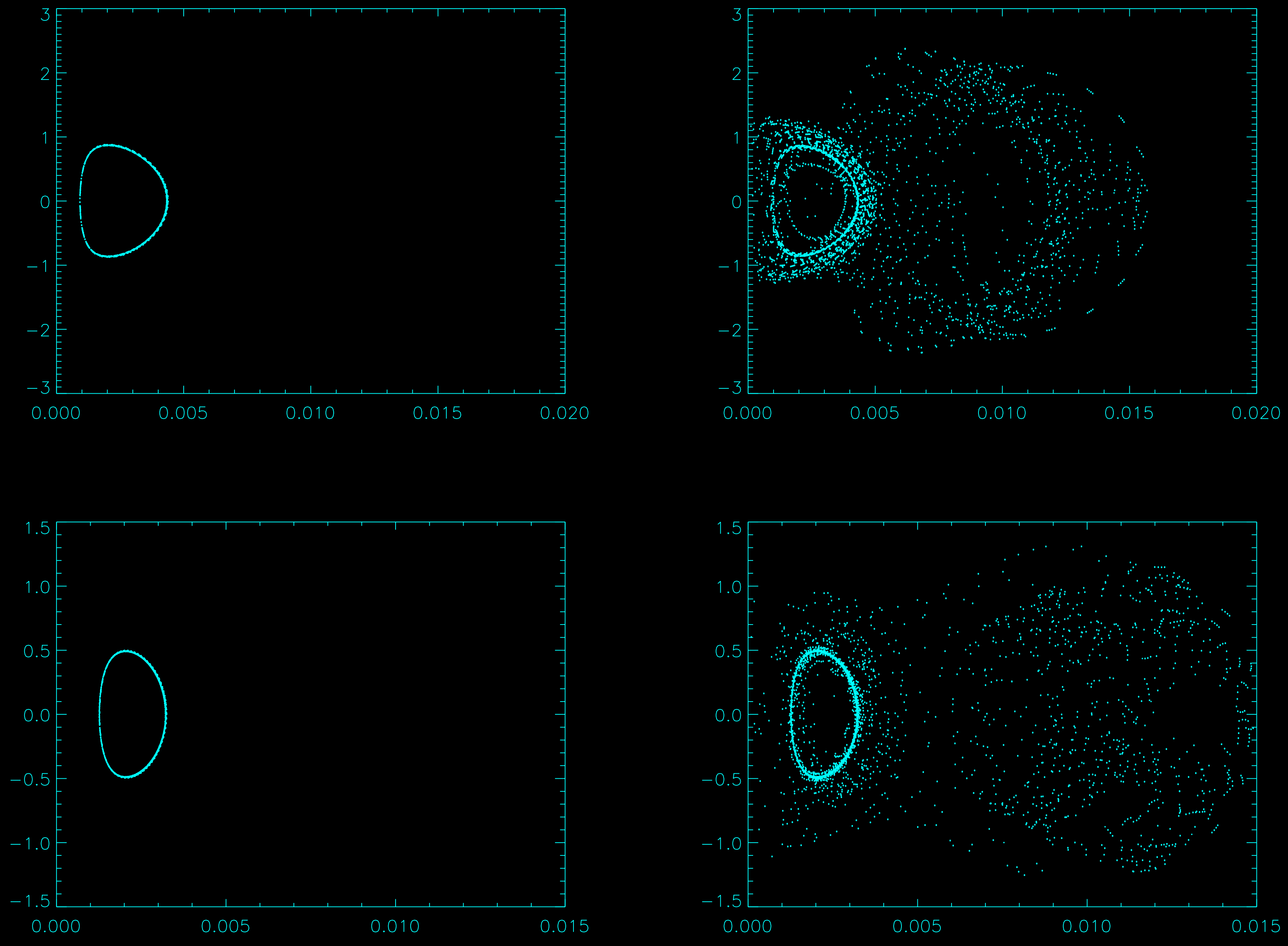

Nonlinear Trapping in the Longitudinal Direction

⇨ Resonant particles and momentum spread are created by nonlinear trapping.

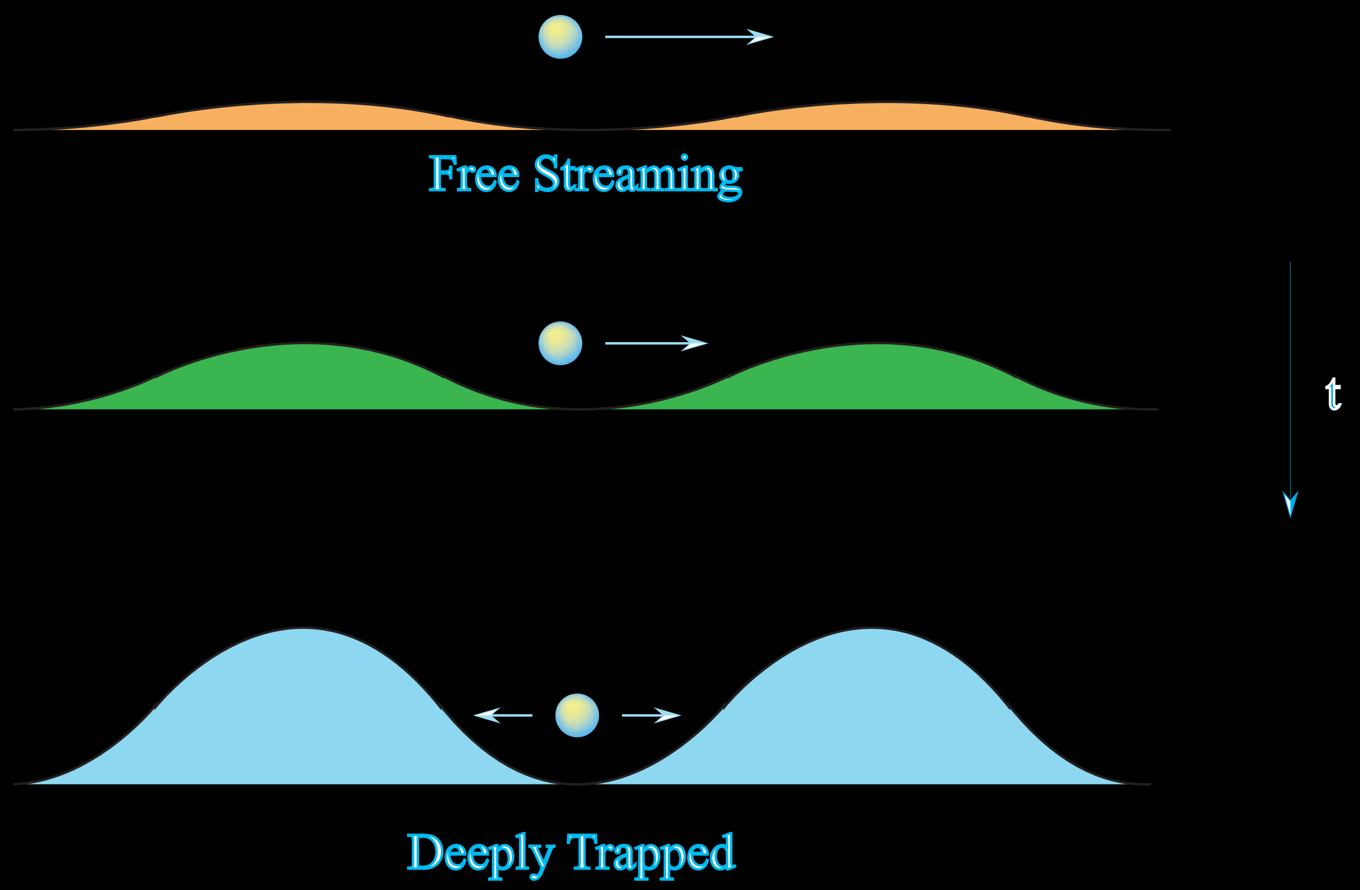

Conclusions: Two-Stream Instability

- A 3D multispecies nonlinear perturbative particle simulation method has been developed to study two-stream instabilities in intense charged particle beams described self-consistently by the Vlasov-Maxwell equations.

- Properties of the two-stream instability are investigated numerically, and are found to be in qualitative agreement with experimental observations and theoretical predictions.
  - The self-consistent simulations show that the most unstable mode of the ion-electron instability has a dipole mode structure.
  - The simulations show that an axial momentum spread and the space-charge induced tune spread provide effective stabilization mechanisms for the two-stream instability.
  - Interesting nonlinear dynamics are observed in the simulations.

Conclusion: Advanced Features of the BEST Code

- Algorithm
  - Nonlinear and linear multispecies simulation based on Vlasov-Maxwell equations.
  - δf low noise particle simulation method.
- Programming: Written in Fortran 90/95 and extensively object-oriented.
- Diagnostics
  - Parallel HDF5 and NetCDF data format for large-scale diagnostics and visualization.
  - Diagnostic tool developed using IDL.
- Parallelization
  - Using OpenMP and MPI on IBM-SP supercomputer at NERSC.
  - Good parallel scaling on 512 processors.
  - Achieved 2.0×10^{11} ion-steps $+\ 4.0 \times 10^{12}$ electron-steps for instability studies.
- Open source and you are welcome to use it: http://nonneutral.pppl.gov/best.htm.

Studies of Two-Stream Instability – Future Plans

- Extend the model to include
  - secondary electron yield;
  - bunching effects.
- Understand nonlinear dynamics of the two-stream instability.
  - Stabilization mechanisms.
  - Mode saturation and secondary nonlinear instability.
  - Ion and electron dynamical response.
- Identify operating regimes and minimize the deleterious effects of the two-stream instability for
  - heavy ion fusion drivers;
  - SNS;
  - and other hight intensity accelerators and storage rings.